



Cite this: DOI: 10.1039/d6sc00998k

All publication charges for this article have been paid for by the Royal Society of Chemistry

Time-resolved spectroscopy of a photoactive dinuclear W/Ru complex: spectroscopic evidence for a metastable intermediate with side-on coordinated carbonyl ligand

Jan-Hendrik Borter,^a Sayan Kangsa Banik,^a Kristian Kunze,^{bc} Stephan Kupfer,^{id *d} Dirk Schwarzer^{*a} and Wolfram W. Seidel^{id *bc}

The photo-induced dynamics of a redox-active dinuclear W(II)/Ru(II) complex, [Tp*W(CO)Br(PyC≡CCH₂)–Ru(bpy)₂](PF₆) (2-PF₆), is revealed by femtosecond infrared and UV-vis pump-probe spectroscopy in combination with quantum chemical calculations. The use of the mononuclear tungsten alkyne complex [Tp*W(CO)Br(PyC≡CCH₃)] (1) as a benchmark allowed an in-depth analysis of the excited state kinetics of 2-PF₆. Excitation of the dinuclear complex at 400 nm produces predominantly a triplet metal-to-ligand charge transfer state localised at the Ru(bpy)₂ chromophore (³MLCT_{bpy}) with a lifetime of 6 ps. The following transformation into a tungsten-centered triplet state (³MC_W) is accompanied by significant charge transfer and rearrangement of the W–C–O geometry. Subsequent intersystem crossing back to the ground state on a timescale of 12 ps produces a vibrationally excited molecule with up to 3 quanta in the CO stretching vibration. A minor fraction of 10% of the population reacts to an intermediate exhibiting a lifetime of 140 ps and a CO stretching frequency of 1703 cm⁻¹. Our quantum chemical calculations disclose that this species corresponds to an isomer trapped in a metastable state of the S₀ potential surface, with the CO bound side-on to the W centre.

Received 4th February 2026
Accepted 6th April 2026

DOI: 10.1039/d6sc00998k

rsc.li/chemical-science

Introduction

Carbon monoxide complexes are a cornerstone of organometallic chemistry.¹ The significance of homoleptic compounds as starting materials can hardly be overestimated. The electrophilic character of the metal-bonded C atom opens up synthetic routes to hydrides and carbene complexes. Migratory insertions of CO in metal-carbon bonds as well as cyclizations with coordinated CO being involved are important elementary steps in catalysis. In this context, carbon monoxide is used as a C₁ feedstock in a variety of processes, which produce value-added base chemicals on mega-tonne scales per annum.² The electronic scope of CO complexes ranges from Ellis' highly reduced carbonyl metallates³ to cationic σ-donor CO complexes presented by Willner and Aubke,⁴ which have recently experienced a renaissance by Krossing and coworkers.⁵ In the gas phase, even homoleptic lanthanide and alkaline earth metal carbonyls have been detected by IR photodissociation spectroscopy by

Zhou, Li and Frenking.⁶ With regard to the Fischer–Tropsch process, lanthanide and uranium complexes and in particular Na₂Cp₂Mg(i) dimers have been proven to be outstanding in direct C–C coupling of several CO molecules by work of the research groups of Cloke,⁷ Arnold,⁸ Liddle,⁹ Evans¹⁰ and Jones.¹¹

The strong preference for end-on C coordination in all these systems based on the frontier orbital composition applies not only to mononuclear but also to polynuclear compounds exhibiting bridging CO. More or less symmetrically carbon bound CO can either reside on an edge (A, Chart 1) or on a surface of a metal cluster (B).¹² With highly oxophilic metals like lanthanides and actinides a dual C,O-end-on mode is regularly observed (C).¹³ An alternative side-on coordination of CO has so far only been found in bimetallic compounds or metal clusters exhibiting a combined end-on/side-on mode, which was originally called linear semi-bridging by Cotton (D).¹⁴

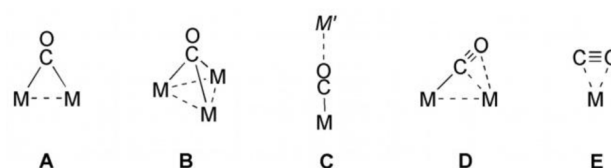


Chart 1 Common bridging modes of CO (A–D) and exclusive side-on coordination mode sought for (E).

^aMax Planck Institute for Multidisciplinary Sciences, Am Fassberg 11, 37077 Göttingen, Germany. E-mail: dschwar@mpinat.mpg.de

^bInstitut für Chemie, Universität Rostock, Albert-Einstein-Straße 3a, 18059 Rostock, Germany. E-mail: wolfram.seidel@uni-rostock.de

^cLeibniz-Institut für Katalyse e.V., Albert-Einstein-Straße 29a, 18059 Rostock, Germany

^dInstitute of Physical Chemistry, Friedrich Schiller University Jena, Helmholtzweg 4, 07743 Jena, Germany. E-mail: stephan.kupfer@uni-jena.de



A closer look at the structural data in dinuclear complexes of type **D** underscores the primacy of end-on coordination. Depending on the type of metals linked and their distance from each other, either the M–C bond¹⁵ or the M–O bond¹⁶ to the side-on bonded metal can be shorter than the other, with both being longer than 2 Å. In contrast, for the CO ligands in compounds of type **D**, the terminal M–C bond is particularly short and falls within the range of less than 2 Å. Apparently, the side-on donor effect from the π_{CO} orbitals and the back-bonding into the π_{CO}^* orbitals by the end-on bound metal constitute a push–pull system, being of crucial relevance for the stability of this motif. Consistently, a mere side-on coordination of the CO ligand to a single metal centre (**E**) is very elusive and has neither been isolated in substance nor detected spectroscopically. This is in stark contrast to the isoelectronic dinitrogen, of which side-on complexes are well known.¹⁷ The non-polar nature of N₂ is an evident reason for this difference, but the exclusive side-on binding is mainly limited to early transition metals, lanthanides, and uranium, and all structurally confirmed N₂ compounds of this type are dinuclear in the $\mu\text{-}\eta^2\text{-}\eta^2$ bonding mode.^{18,19} Significantly, this bonding mode is particularly activating,^{19,20} which makes side-on CO complexes an intriguing intermediate. In addition, linkage isomerism in complexes of the related nitric oxide is subject of spectroscopic investigations and studies by photocrystallographic techniques for some time.^{21,22} Recently, side-on nitrosyl complexes were presented, which are structurally characterized and stable at ambient temperature.²³

Investigations into the excited state dynamics of carbonyl complexes after UV light irradiation are among the early topics of classical photochemistry seeking a rationale for corresponding synthetic procedures.²⁴ The photodissociation of one CO ligand in homoleptic transition metal carbonyls were shown to proceed in a fs time frame, and the rearrangement of the polyhedra in different spin states as well as potential solvent adducts were extensively studied.²⁵ Surprisingly, there are no reports on the spectroscopic observation of intermediates with side-on coordination of the CO ligands leaving or remaining in the complex. However, more recently theoretical work describing species with side-on CO coordination at least as minima on the hypersurface has attracted attention.²⁶

As part of our investigations into electron transfer cascades for light-driven charge separation, we have constructed dinuclear complexes, in which the metals are linked by a pyridyl propargyl ligand. The alkyne complex **1** equipped with a pyridine and a methyl substituent (Fig. 1) can act as cyclometalating C,N-chelate ligand mimicking the binding behaviour of

phenylpyridine (ppy), which is used as a cyclometalating monoanionic ligand in many photoactive Ir(III) compounds. The present W(II) alkyne complex as a metalla-ligand exhibits additionally a reversible redox process at a potential of about 0 V *vs.* the Fc/Fc⁺ couple, which is capable of reductive quenching of an excited triplet ³MLCT transition state at either Ru(II) or Ir(III), respectively. The synthesis and spectroscopic characterization of the mononuclear complex **1** and the corresponding dinuclear compounds **2**-PF₆ and **3**, including the elucidation of the molecular structures by single crystal XRD and electrochemical studies, are subject of a preceding publication.²⁷ The determined redox potentials as well as the significant fluorescence quenching in relation to the parent compounds [(bpy)₂Ru(ppy)](PF₆) and [Ir(ppy)₃] indicate a fast intramolecular electron transfer. To uncover the photodynamic behaviour in depth, transient UV-vis as well as transient IR (TRIR) absorption spectroscopy with the Ru-congener **2**-PF₆ and **1** as mononuclear benchmark were performed in a fs to ps time regime. These experimental investigations are supported by scalar-relativistic time-dependent density functional theory (SR-TDDFT) simulations to elucidate the Franck–Condon photophysics and intersystem crossing (ISC) pathways as well as spectral signatures of photoexcited intermediates of **2**-PF₆. Finally, the synergic synthetic-spectroscopic-theoretical approach allowed to unravel the subsequent excited state relaxation channels associated with electron transfer *vs.* energy transfer. For the first time, we succeeded in spectroscopically detecting a side-on CO complex as an intermediate. Herein, we report on the results of these investigations.

Results and discussion

The alkyne complex **1** was prepared starting from [Tp*W(CO)₃] and 2-propynylpyridine. Deprotonation of **1** by KOtBu in the presence of [(bpy)₂Ru(PPh₃)Cl]PF₆ provided **2**-PF₆, which was obtained analytically pure by chromatography and subsequent crystallization. The dark-blue compound exists as an individual diastereomer, which is stable for month under daylight.²⁷

To elucidate the photo-induced excited state dynamics in complexes **1** and **2**-PF₆ we applied femtosecond pump-probe spectroscopy. Pump pulse-induced ($\lambda_{\text{exc}} = 400$ nm) absorption changes were monitored in the UV-vis at 350–730 nm using white-light continuum pulses and in the region of the carbonyl stretching frequency (1600–2200 cm⁻¹) using IR probe pulses with a bandwidth of about 200 cm⁻¹ (details about the experimental setup are presented in a recent publication²⁸ and in the SI).

Mononuclear tungsten complex 1

The absorption spectrum of **1** shows weak bands at 670 and 410 nm, and a stronger one at 280 nm (see black line in Fig. 2, upper panel), which were assigned to W-centred d–d, W-to-pyridine, and W-to-Tp* singlet transitions, respectively.²⁷ Pump pulse excitation at 400 nm leads to positive transient absorption over the whole UV-vis range (Fig. 2, upper panel). Its decay is reasonably well fitted by a sum of two exponentials with a dominant contribution exhibiting a time constant of $\tau_2 = 7$ ns

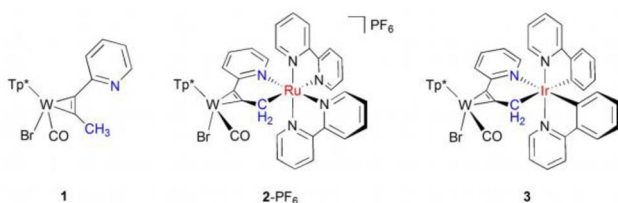


Fig. 1 Mono- and dinuclear complexes under study.



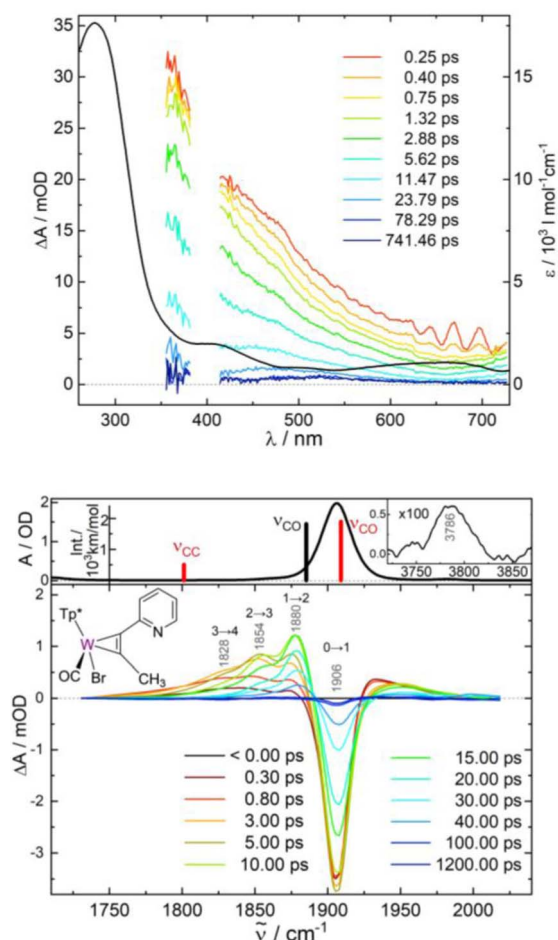


Fig. 2 Absorbance changes (ΔA) in units of milli optical density (mOD) induced by 400 nm excitation of the tungsten complex **1** in acetonitrile at pump-probe delays as indicated. Upper panel: transients in the UV-vis (regions distorted by the pump pulse are cut out); the black line represents the absorption spectrum (extinction coefficient: right vertical axis). Lower panel: transient IR difference spectra for the CO stretching vibration; the upper insets display the stationary IR spectrum with the fundamental CO transition at $\nu_{01} = 1906 \text{ cm}^{-1}$ and the first overtone at $\nu_{02} = 3786 \text{ cm}^{-1}$. Stick spectra show calculated frequencies at the B3LYP/def2-SVP level of theory for the ground state (black) and the relaxed T_1 state of mixed ${}^3\text{MC}_W/{}^3\text{MLCT}$ character (red).

1 ps and a minor one of $\tau_1 = 0.25 \pm 0.1$ ps. Transient IR spectra for complex **1** are presented in the lower panel of Fig. 2. The upper insets show the FTIR spectrum of **1** with the fundamental CO stretching vibration at $\nu_{01} = 1906 \text{ cm}^{-1}$ and an enlarged image of its overtone absorption at $\nu_{02} = 3786 \text{ cm}^{-1}$. Directly after 400 nm excitation the ground state absorption of the CO stretching vibration is bleached and broad almost featureless positive red- and blue-shifted absorptions arise. At pump-probe time delays of 0.3–3.0 ps two bands at 1880 and 1854 cm^{-1} and a shoulder at 1828 cm^{-1} emerge. The frequency spacing between these features, as well as the difference between the 1880 cm^{-1} band and the bleached ground state transition at $\nu_{01} = 1906 \text{ cm}^{-1}$, coincide with the anharmonicity of the CO stretching mode determined from the static IR spectrum: $2\omega_e x_e = \nu_{02} - 2\nu_{01} = -26 \text{ cm}^{-1}$ ($\nu_{02} = 3786 \text{ cm}^{-1}$, see Fig. 2). Therefore,

we attribute the absorption bands at 1880, 1854, and 1828 cm^{-1} to $\nu = 1 \rightarrow 2$, $2 \rightarrow 3$, and $3 \rightarrow 4$ transitions of the CO stretching mode in the electronic ground state, respectively. Their appearance in less than 0.3 ps indicates excited state lifetimes of less than a few hundred fs, leading to rapid recovery of the ground state. Excited vibrational population in the CO-stretching mode was previously observed in ground state $\text{M}(\text{CO})_5(n\text{-hexane})$ ($\text{M} = \text{Cr}, \text{Mo}, \text{W}$) produced by photodissociation of $\text{M}(\text{CO})_6$.²⁹

This assignment to a vibrationally hot electronic ground state species is consistent with the UV-vis transients of Fig. 2. In general, thermal excitation of a molecule leads to broadening of its electronic transitions with absorption being reduced in its centre and enhanced at the low energy side.³⁰ The ground state spectrum of **1** is dominated by the relatively strong absorption band at 280 nm. It is conceivable that its thermally induced broadening superimposes any bleaching in the centre of the weak 410 and 670 nm bands resulting in entirely positive absorption changes similar to the UV-vis transients of Fig. 2. Therefore, the dominant decay component of $\tau_2 = 7 \pm 1$ ps can be safely assigned to vibrational cooling – a typical value for a large polyatomic molecule in solution.^{31,32} The minor contribution with $\tau_1 = 0.25 \pm 0.1$ ps could be due to a short-lived excited state species, most likely the T_1 state of **1**. According to our quantum chemical calculations performed at the density functional level of theory (DFT, B3LYP/def2-svp; see Fig. S3 in the SI for details), this T_1 state is of triplet metal-centred/metal-to-ligand charge transfer character (*i.e.* ${}^3\text{MC}_W/{}^3\text{MLCT}$), while the reduced π -back-bonding leads to a slight elongation of the W–CO bond (2.030 Å) with respect to the singlet ground state (1.965 Å). Spectroscopically, the altered electronic structure, *i.e.* in the vicinity of the W–CO motif, results in the blue-shift of the CO stretching mode from 1885 cm^{-1} (S_0) to 1909 cm^{-1} within T_1 (see inset in the lower panel of Fig. 2). Assuming a short-lived T_1 , from which fast intersystem crossing (ISC) to the ground state (T_1-S_0 gap in ${}^3\text{MC}_W$ is only 0.25 eV) occurs, would be consistent with the feature seen for the IR transients at 1930 cm^{-1} at early times. The lifetime in the primary populated singlet manifold appears to be below the time resolution of our UV-vis pump-probe spectrometer of about 70 fs.

Population in high ν -states of the CO stretching mode evidenced by the IR transients of Fig. 2 indicates a highly non-statistical energy distribution within the molecule after return to the ground state. Note, that based on the frequencies computed from DFT (see Table S2 in the SI) the internal vibrational temperature of **1** after 400 nm photon energy uptake and its statistical distribution over all modes in the ground state would correspond to $T_{\text{exc}} \sim 630 \text{ K}$ – too low to produce any appreciable population in excited ν -states of the CO stretching vibration. A non-statistical distribution with high energy in this mode can be generated by considering the significant MLCT character of the excited state, which shifts electron density away from the metal to the aromatic ligands. This partially depletes antibonding π^* orbitals of the carbonyl ligand. Consequently, the CO bond begins to relax from the Franck–Condon region towards the new equilibrium geometry with contracted CO bond. Apparently, the system notably evolves in this direction



before it hops back to the ground state surface leaving the CO bond vibrationally excited when now attempting the ground state equilibrium geometry. Non-statistical vibrational populations produced by electronic excitation and ultrafast ground state repopulation have been observed for other tungsten carbonyl complexes before.^{29,31}

We fitted the dynamics of the CO stretching vibration by a kinetic model shown in the left panel of Fig. 3. After photo excitation and fast ISC the T_1 state is populated from which transfer into excited ν -states of the CO mode in the ground state occurs. The rate constants k_n are controlling the lifetime of the T_1 state and the resulting ground state vibrational population distribution, G_n . The ground state relaxation is treated within perturbation theory giving downwards one-quantum transition rate constants of $k_{n,n-1} = n k_{10}$; ($n = 1, 2, \dots$)³³ where k_{10} is the relaxation rate constant for a transition $\nu = 1 \rightarrow 0$ of the CO stretching mode. The time-dependent concentrations obtained from the kinetic model are translated into IR difference spectra based on the harmonic approximation giving a linear dependence of the cross section for absorption and stimulated emission on the vibrational quantum number³⁴ (the details of this procedure are presented in the SI).

We find good agreement between calculated and measured IR difference spectra when the k_n values are adjusted to produce approximately a Boltzmann distribution at $T_{\text{vib}} = 4500 \pm 500$ K within the ν -states of the CO stretching mode and the vibrational lifetime is set to $\tau_{10} = 1/k_{10} = 13 \pm 1$ ps (see right panel in Fig. 3, details are described in the SI). At early times the modelled spectrum overestimates the modulations caused by populated higher vibrational quantum states of the CO stretching mode. This can be explained by the fact that the model neglects additional shifts caused by off-diagonal coupling to other excited vibrational modes in the molecule, which would lead to additional absorption lines washing out the modulation.³⁴ At pump-probe delays >5 ps the agreement between calculated and measured spectra is excellent. The vibrational distribution created after $T_1 \rightarrow S_0$ ISC corresponds to an average energy in the CO stretching vibration of $\langle E \rangle_{\text{CO}} \cong 1560 \text{ cm}^{-1}$, indicating that 6% of the applied photon energy flows into this mode when the ground state is repopulated.

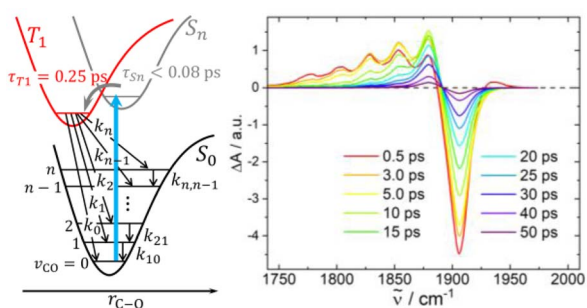


Fig. 3 Left panel: kinetic model describing the dynamics of complex 1 after photoexcitation. Rate constants k_0 to k_n determine repopulation of the electronic ground state by intersystem crossing into corresponding ν -states of the CO stretching mode; k_{10} to $k_{n,n-1}$ are vibrational relaxation rate constants. Right panel: simulated spectral evolution (see text).

Since the CO stretching frequency is rather high, its coupling to the solvent is weak. Therefore, the observed energy loss ($\tau_{10} = 13$ ps) is likely to be determined by intramolecular vibrational redistribution (IVR) to low frequency modes of the molecule, from where it flows into the solvent. This scenario is consistent with the vibrational cooling time of 7 ps, which was derived from the decay of the UV-vis transients, since the postulated broadening of the 280 nm absorption band is likely caused by other excited ground state vibrations than the CO stretching mode.

In summary, following 400 nm excitation, complex 1 undergoes fast ISC to the T_1 state with a lifetime of ~ 0.25 ps. Subsequent repopulation of the ground state produces a highly non-statistical vibration energy distribution where a significant amount of the photon energy flows into the CO stretching vibration of the molecule. Its transfer to low frequency modes of the molecule happens on a timescale of 13 ps.

Dinuclear tungsten–ruthenium complex 2-PF₆

UV-vis spectrum. The UV-vis absorption spectrum of 2-PF₆ is dominated by ¹MLCT transitions of the Ru(bpy)₂-based chromophore (Fig. 4a).²⁷ Quantum chemical calculations (TD-B3LYP/def2-svp) enable to assign the underlying electronic transitions to six dipole-allowed singlet ¹MLCT_{bpy} excitations (into S_7 – S_{10} , S_{13} and S_{14}) between 536 and 441 nm (2.31–2.81 eV). Notably, S_7 and S_{10} feature a minor metal-to-metal charge transfer (MMCT) character whereby electron density is partially shifted from the t_{2g} orbitals of Ru to the vacant d orbitals of the W(II) centre. In addition, and in a similar fashion as observed previously for 1, a weakly dipole-allowed ¹MC_W transition (into S_1) of the tungsten moiety is predicted at 719 nm (1.72 eV). Further details with respect to the electronic transitions involved in the Franck–Condon region are summarised in the SI (see Fig. S5a and Tables S3 and S4).

Pump-probe spectroscopy. As shown in Fig. 4a, excitation at 400 nm leads to immediate bleaching of the strong 550 nm absorption band attributed to Ru-to-bpy ¹MLCT transitions. Superimposed excited state absorptions produce maxima at 360, 430, and >730 nm. Apart from an instant initial rise, all time traces for the excited state absorptions (Fig. 4b–e) reveal an additional increase on a timescale of ~ 0.25 ps. Subsequently, the 360 nm and 730 nm bands decay with a time constant of ~ 13 ps, whereas the 430 nm feature exhibits a further significant rise within ~ 4 ps before decaying parallel to the other excited state absorptions. The picosecond time constants were found again in the bleach signal, where the 4 ps and 13 ps components are responsible for 48% and 23% of its recovery, respectively. An additional contribution to the ground state recovery of 10% has a time constant of ~ 180 ps.

The underlying dynamics are revealed in more detail by the IR transients of Fig. 5 showing well separated absorption features (panel c) and their time evolution (panels d–g), respectively. The photo-induced ground state bleach of the CO fundamental absorption at 1884 cm^{-1} in Fig. 5c is accompanied by two blue-shifted absorptions: a stronger one at 1904 cm^{-1} and a weaker shoulder at 1945 cm^{-1} . The following decay of the



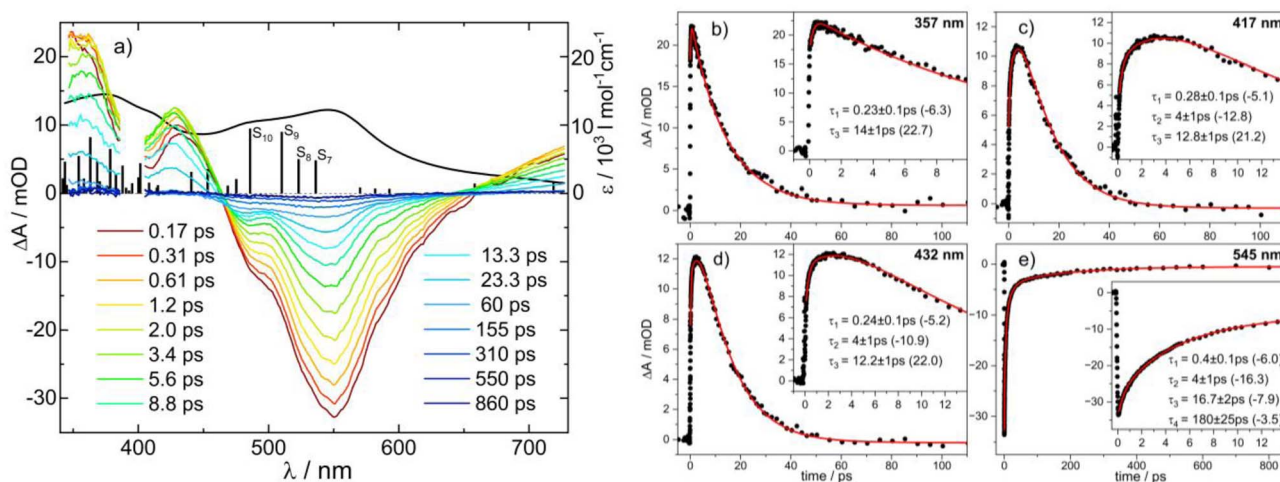


Fig. 4 (a): UV-vis transient difference spectra of the W-Ru complex 2-PF₆ in acetonitrile after 400 nm excitation at pump-probe delays as indicated (regions distorted by the pump pulse are cut out); the black line represents the ground state absorption spectrum (extinction coefficient: right vertical axis); stick spectrum: calculated electronic transitions (TD-B3LYP/def2-svp). (b)–(e): Time traces for selected probe wavelengths with multi-exponential fits (red lines; inserts zoom into the initial phase of the dynamics and show time constants with corresponding amplitudes in brackets).

1904 cm⁻¹ absorption is associated with a further rise of the 1945 cm⁻¹ band. Since these processes are exhibiting similar time constants of $\tau_1 \cong 6$ ps, we tentatively attribute these bands to CO stretching vibrations of the W-Ru complex in two different states (T₂ and T₁, respectively) and the observed kinetics to a corresponding transformation of T₂ into T₁. A change in the CO bands by 20–60 cm⁻¹ to higher frequencies is found in a comparable manner for excited ³MLCT states of related Re^I(CO)₃ complexes.³⁵ Subsequently, the 1945 cm⁻¹ feature disappears ($\tau_2 \cong 12$ ps) and the electronic ground state,

G, recovers suggesting a reaction T₁ → G. Similar to complex 1, ground state recovery leaves the molecule with population in excited states of the CO stretching mode with vibrational transitions at 1884 ($\nu = 0 \rightarrow 1$), 1858 ($\nu = 1 \rightarrow 2$), 1832 ($\nu = 2 \rightarrow 3$), and 1808 cm⁻¹ ($\nu = 3 \rightarrow 4$). Note, that the anharmonic shift of -26 cm⁻¹ for the CO stretching mode coincides with the value found for 1.

Interestingly, the decay of the T₁ band also correlates with formation of an absorption feature at 1703 cm⁻¹ (rise time ~12 ps). Clearly, the onset of its rise is slightly delayed with an

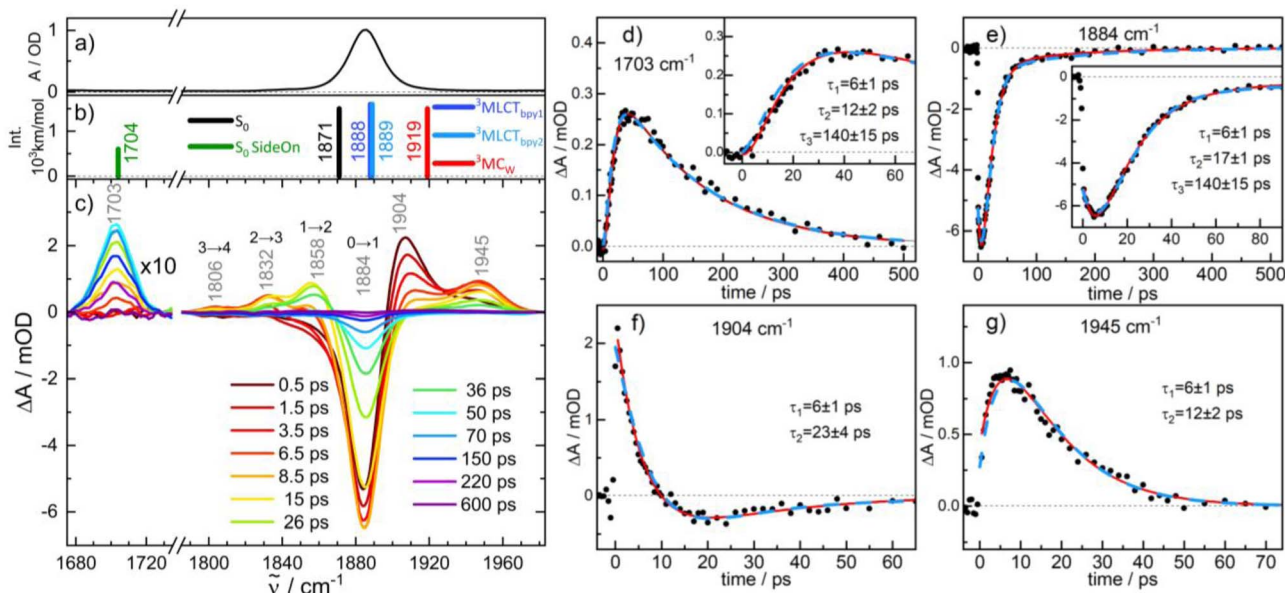


Fig. 5 (c) IR transient difference spectra for the CO stretching mode of complex 2-PF₆ in acetonitrile after 400 nm excitation at pump-probe delays as indicated (the region below 1740 cm⁻¹ is 10× enlarged); panels (a) and (b) display the FTIR spectrum and calculated stick spectra for various intermediates. (d)–(g) Time evolution of selected transient IR absorption features with exponential fits (red lines with corresponding time constants); dashed blue lines are time traces from the kinetic model of Fig. 7.



induction period ~ 6 ps suggesting that the growth of the 1703 cm^{-1} band is associated with the decay of T_1 and not T_2 . The lifetime of this intermediate I of $\tau_3 \cong 140$ ps agrees with a $\sim 10\%$ component in the ground state recovery of the $\nu = 0 \rightarrow 1$ transition at 1884 cm^{-1} , suggesting that the 1703 cm^{-1} mode of I corresponds to a CO stretching vibration as no other transient absorption features in the range $1650\text{--}2200\text{ cm}^{-1}$ were detected.

Note, that we were unable to detect an IR absorption peak at around 1700 cm^{-1} for complex **1**. This is consistent with the observation that, during the recovery of the ground state of **1**, the bleaching of the $\nu = 0 \rightarrow 1$ transition is always balanced by red-shifted positive absorptions from excited CO vibrational states. However, for **2-PF₆**, these excited state bands are absent during the lifetime of I (see Fig. S7 in the SI).

Assignment of the intermediates T_2 and T_1 . Excitation of the parent complex $[\text{Ru}(\text{bpy})_3]^{2+}$ at around 400 nm is well known to populate a $^3\text{MLCT}$ state within 40 fs via intersystem crossing from the singlet manifold. The $^3\text{MLCT}$ absorption spectrum shows a shallow, broad absorption in the red and an intense peak at 360 nm .³⁷ The latter is attributed to a transition in the reduced bipyridine ligand. The absorption features observed in the initial UV-vis transients displayed in Fig. 4a are strikingly similar to those exhibited by photoexcited $[\text{Ru}(\text{bpy})_3]^{2+}$. This observation leads us to conclude, that after excitation of **2-PF₆**, a Ru-centered $^3\text{MLCT}$ state is populated within our experimental time resolution. The $^3\text{MLCT}$ state is therefore also responsible for the CO absorption band of the T_2 state at 1904 cm^{-1} , which appears directly after the pump pulse (Fig. 5c).

This assignment is further supported by quantum chemical calculations within the framework of unrestricted DFT and TDDFT (see details in SI). The first three lowest energy triplet states in the Franck-Condon geometry are a tungsten-centred ($^3\text{MC}_w$, T_1) and two energetically close Ru(bpy)₂-based metal-to-ligand CT states ($^3\text{MLCT}_{\text{bpy}1}$ and $^3\text{MLCT}_{\text{bpy}2}$, T_2 and T_3), where charge density is transferred to one or the other bpy ligands (charge density difference plots are shown in Fig. 6).

After geometry optimization the $^3\text{MLCT}_{\text{bpy}}$ states feature almost identical CO stretching frequencies of 1888 and 1889 cm^{-1} , which are slightly blue-shifted by $\sim 18\text{ cm}^{-1}$ with respect to the S_0 ground state ($\nu_{\text{CO}} = 1871\text{ cm}^{-1}$, see Fig. 5b). As the spectroscopic signatures of the two quasi-isoenergetic $^3\text{MLCT}_{\text{bpy}}$ states are almost similar, it is not possible to clarify whether both states coexist or only one dominates. Hence in our discussion we treat the two as a single species.

The relatively small change in CO stretching frequency reflects the fact that in the $^3\text{MLCT}_{\text{bpy}}$ state the electronic and structural environment around the tungsten is quite similar to that in the S_0 state, causing e.g. only a marginal stretching of the W-CO bond from 1.958 \AA (S_0) to 1.968 \AA ($^3\text{MLCT}_{\text{bpy}}$). The calculated frequency shift agrees well with the experimental S_0 - T_2 blue shift of 20 cm^{-1} , which confirms the assignment of the 1904 cm^{-1} band to the $^3\text{MLCT}_{\text{bpy}}$ state. The appearance of the $^3\text{MLCT}_{\text{bpy}}$ state within the time resolution of our experiment is consistent with scalar-relativistic (SR)-TDDFT simulations yielding sizeable spin-orbit couplings of up to 248 cm^{-1} along

these $^{1/3}\text{MLCT}_{\text{bpy}}$ gateway states (see Table S5), which is within the typical range for 4d transition metal complexes.^{38,39}

By contrast, the $^3\text{MC}_w$ state undergoes major W-CO bond elongation during relaxation to 2.024 \AA (see table in Fig. 7), resulting in a CO stretching frequency of 1919 cm^{-1} , i.e. 48 cm^{-1} higher compared to the S_0 state. As this compares well with the experimentally observed value for species T_1 (61 cm^{-1}), we attribute the transient CO band at 1945 cm^{-1} to the $^3\text{MC}_w$ state.

The $^3\text{MLCT}_{\text{bpy}} \rightarrow ^3\text{MC}_w$ population transfer suggested by the kinetics of the transient IR bands at 1904 and 1945 cm^{-1} may be viewed as an energy transfer or a dual mutual electron transfer from the $^3\text{MLCT}_{\text{bpy}}$ donor (D) to the $^3\text{MC}_w$ acceptor (A) state, where the corresponding rate constant k can be calculated from semi-classical Marcus theory:

$$k = \frac{2\pi}{\hbar} |V_{\text{DA}}|^2 (4\pi\lambda k_{\text{B}}T)^{-1/2} \exp\left(-\frac{(\Delta G + \lambda)^2}{4\lambda k_{\text{B}}T}\right) \quad (1)$$

In eqn (1) V_{DA} denotes the electronic coupling between D and A at the crossing point of the diabatic potential energy surfaces, λ is the reorganization energy, and ΔG represents the driving force, i.e. the Gibbs free energy, for the process. Notably, recent theoretical investigations have shown that such Marcus-adapted formalism allows to predict not only electron transfer but also the kinetics of (Dexter-type) energy transfer processes.³⁸⁻⁴⁰ We estimated the rate constant – associated with energy transfer – based on diabatic potentials derived from a linearly interpolated internal coordinate connecting the optimized equilibrium structures of the $^3\text{MLCT}_{\text{bpy}1}$ and $^3\text{MC}_w$ states (resulting in $\Delta G = -0.60\text{ eV}$ and $\lambda = 0.76\text{ eV}$), and applied the minimum splitting method^{38,41} to determine the electronic coupling of $V_{\text{DA}} = 5.5\text{ meV}$ at the crossing point (see the SI for details). The calculated lifetime of $k^{-1} = 2.4\text{ ps}$ agrees well with the measured time constant of $\tau_1 = 6\text{ ps}$ associated with the $^3\text{MLCT}_{\text{bpy}} \rightarrow ^3\text{MC}_w$ conversion and confirms the character of this population transfer.

The major decay channel for the $^3\text{MC}_w$ state appears to be ISC to the electronic ground state. We calculate a spin-orbit coupling of 1440 cm^{-1} between the two states consistent with fast relaxation. Notably, the $^3\text{MC}_w$ - S_0 energy gap in $[2]^+$ is with 0.44 eV almost twice as big as in **1**, which indicates less efficient deactivation in the dinuclear complex.

Taking into account the simulated electronic spectra obtained from TDDFT (see Fig. S5 and S6a in the SI), the reaction cascade $^3\text{MLCT}_{\text{bpy}} \rightarrow ^3\text{MC}_w \rightarrow S_0$ derived from the IR transients is fully consistent with the time-resolved UV-vis data of Fig. 4. The 4 ps rise time observed at probe wavelengths of 430 and 550 nm is close to $\tau_1 = 6\text{ ps}$, suggesting its origin in the $^3\text{MLCT}_{\text{bpy}} \rightarrow ^3\text{MC}_w$ transformation. In fact, the calculated cross sections of the $^3\text{MC}_w$ state at these wavelengths are larger than for the $^3\text{MLCT}_{\text{bpy}}$ state. This leads to an increase in excited state absorption at 430 nm and to a significant bleach recovery at 550 nm as this reaction proceeds. Furthermore, the final decay time constant of all UV-vis excited state absorptions is close to $\tau_2 \cong 12\text{ ps}$ – in agreement with the $^3\text{MC}_w$ lifetime determined from



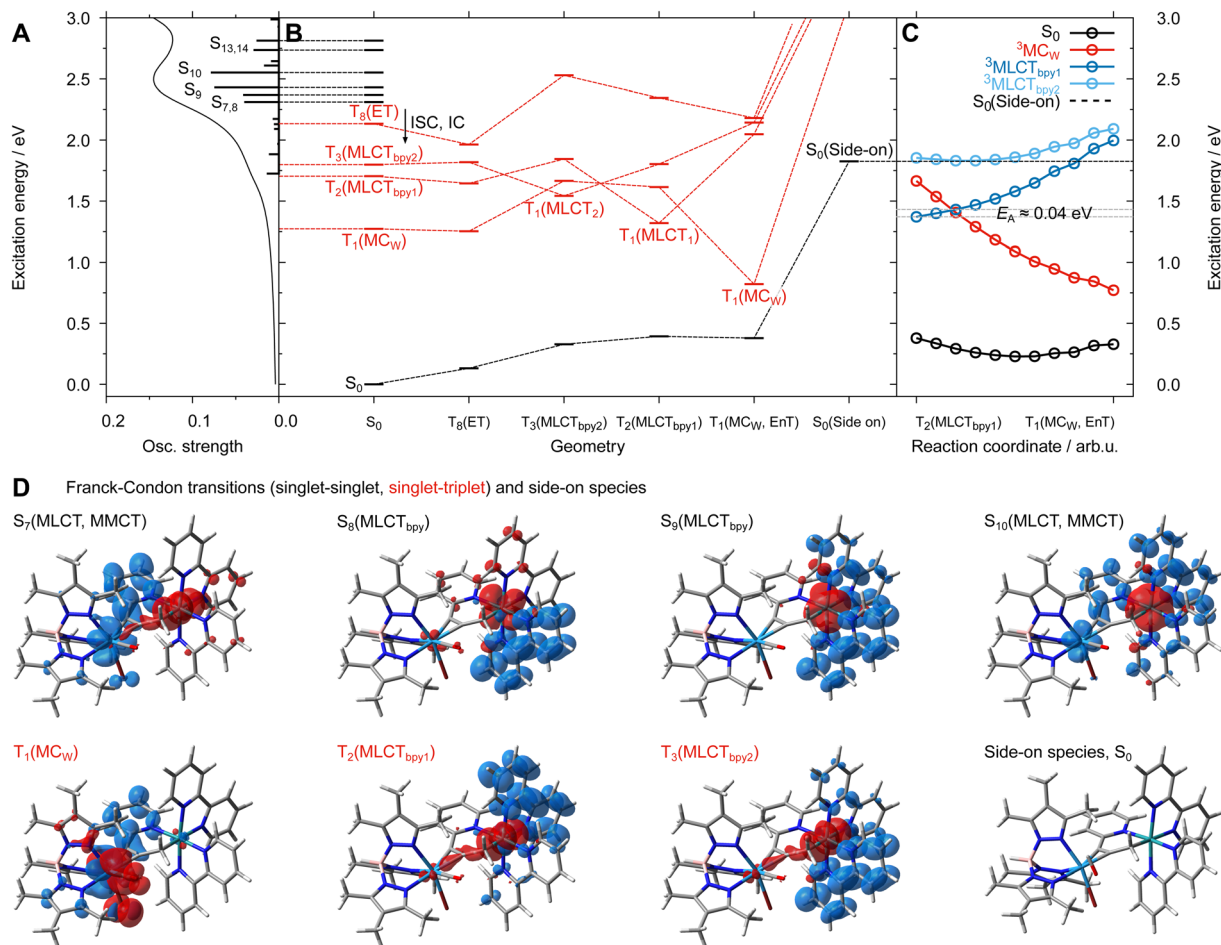


Fig. 6 (A): Simulated electronic absorption spectrum of $[2]^+$. Prominent dipole-allowed singlet transitions are indicated. (B): Excited-state relaxation scheme involving the initially populated singlet states (in black) and low-lying triplet states (in red) accessible upon intersystem crossing (ISC) and internal conversion (IC) to the ${}^3\text{MLCT}_{\text{bpy}}$ states (T_3 and T_2) and the lowest triplet state of ${}^3\text{MC}_W$ character as well as the singlet side-on species. (C): Potential energy curves connecting the equilibrated lowest energy ${}^3\text{MLCT}_{\text{bpy1}}$ state (dark blue) and the ${}^3\text{MC}_W$ (red) minima; an activation energy of merely 0.04 eV is predicted. (D): Electronic characters of key transitions are visualised by means of charge density difference plot (charge transfer from red to blue) and fully equilibrated side-on species.

the IR transients. Finally, the two data sets exhibit a 140–180 ps process, which is responsible for $\sim 10\%$ of the ground state recovery. The origin of this kinetic component is discussed in the next section.

Nature of the intermediate I. The temporal evolution of the 1703 cm^{-1} band for intermediate I shows three main characteristics, *i.e.* (i) delayed response of about 6 ps with respect to the excitation pulse, (ii) subsequent 12 ps rise, which is similar to the lifetime of the T_1 state, and (iii) final decay with time constant $\tau_3 \approx 140$ ps. Observation (i) and (ii) suggest a reaction path $T_1 \rightarrow \text{I}$. Since τ_3 correlates with a corresponding ground state recovery component of 10%, and no other absorption band was detected in the $1650\text{--}2200\text{ cm}^{-1}$ region that could account for the bleached intensity at 1884 cm^{-1} , we investigated the possibility that the 1703 cm^{-1} feature is a CO stretching vibration although the observed red shift of 181 cm^{-1} relative to S_0 appears rather large. Interestingly, similar strong downshifts have been observed for photogenerated nitrosyl complexes, where the NO ligand bound to a transition metal undergoes

a transformation from a linear to a side-on geometry (see *e.g.* review Bitterwolf²² and references cited therein), suggesting that in I the carbonyl might be bound in a side-on (η^2) mode.

Our DFT calculations indeed confirm the existence of a metastable isomer of $[2]^+$ on the S_0 potential surface, with the CO bound side-on to the W centre. The energy of this isomer is 1.82 eV above the global minimum, *i.e.* it is accessible by the applied photon energy of $E_{\text{exc}} = 3.10$ eV. The complex exhibits a CO stretching frequency of 1704 cm^{-1} , which is in excellent agreement with the experimental value of 1703 cm^{-1} . According to our calculations is the side-on species notably higher in energy than the ${}^3\text{MC}_W$ state (Fig. 6B and C) prohibiting a population transfer from the relaxed ${}^3\text{MC}_W$ to the side-on ground state. This points to a deficiency in the calculations, as the transformation $T_1 \rightarrow \text{I}$ is clearly evident in the experiment.

We also checked an alternative hypothesis where I corresponds to a fragment generated by cleavage of the W–CO bond in complex $[2]^+$. In this scenario the free CO molecule is spectroscopically silent due to its low IR cross section and broad



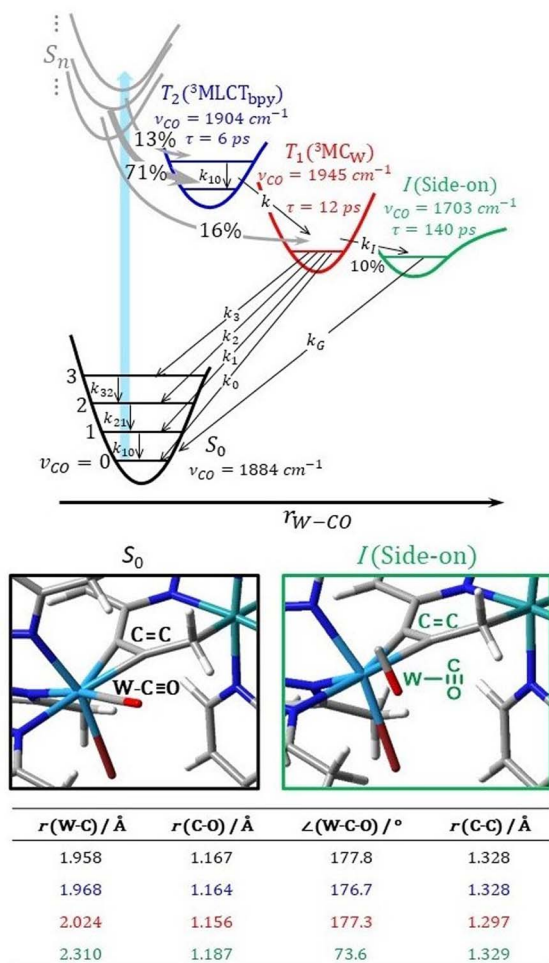


Fig. 7 Kinetic model describing the dynamics of complex 2-PF₆ after photoexcitation (blue arrow) and fast ISC (grey arrows). Within time resolution the states T₂ and T₁ are populated in a ratio 0.84 : 0.16; T₂ transforms into T₁ with rate constant k ; T₁ reacts to the CO side-on complex I (rate constant k_1) or CO stretching mode excited ground state molecules (rate constants k_0 to k_3); k_{10} to k_{32} are vibrational relaxation rate constants; k_G determines the lifetime of I. Structural parameters of the W–CO moiety and the propargyl C=C bond length are indicated (black: S₀, blue: ³MLCT_{bpy}, red: ³MC_W, green: side-on); see zoomed in tungsten coordination environment within the singlet ground state and the side-on species. DFT-optimised equilibrium structures are available *via* the free online repository Zenodo (see SI).

absorption band in solution,⁴² and the 1703 cm⁻¹ feature would correspond to the C=C stretching vibration of the alkyne ligand in the fragment. Its complete decay and recovery of the ground state bleach would also imply 100% geminate recombination of the free CO with the fragment on a timescale of 140 ps. In our calculations, however, we find a W–CO bond dissociation energy of 2.31 eV indicating that this reaction path is energetically even more demanding than formation of the side-on complex (at 1.82 eV). Furthermore, in the fragment the C=C stretching vibration is too low in frequency ($\nu_{\text{CC}} = 1617 \text{ cm}^{-1}$) and not intense enough to account for the observed strength of the 1703 cm⁻¹ band (*e.g.* ν_{CC} in Fig. S4). The insertion of CO into the neighbouring bonds was also considered as a potential

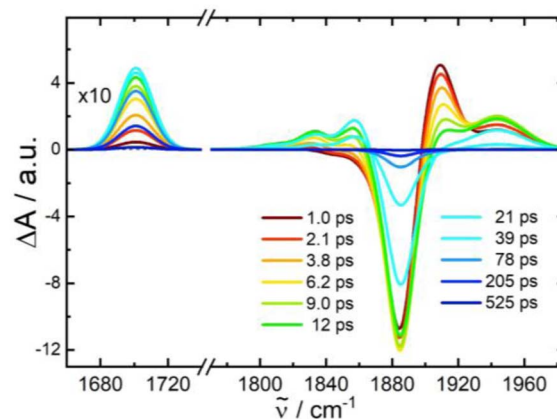


Fig. 8 Simulated spectral evolution of IR difference spectra applying the kinetic model of Fig. 7 (for details see text).

alternative. While a halocarbonyl ligand is extremely rare and unlikely,⁴³ complexes of the C(O)C(R)C(R) building block are known.⁴⁴ However, respective CO vibrations were observed between 1650 and 1670 cm⁻¹. Furthermore, our DFT calculations on a putative species of [2]⁺ did not even yield a minimum on the hypersurface. This result is plausible given the 16 valence electron count of the hypothetical species. Thus, we conclude that the intermediate I corresponds to a metastable side-on complex which is formed *via* the non-equilibrated ³MC_W state with an activated W–CO bond.

Kinetic model for the excited state dynamics of 2-PF₆. The temporal evolution of the IR transients in Fig. 5 and their assignment by our quantum chemical calculations (Fig. 6) suggest an excited state relaxation mechanism, shown in Fig. 7, where the absorption features at 1904, 1945, and 1703 cm⁻¹ are attributed to the intermediates T₂₍₃₎(³MLCT_{bpy}), T₁(³MC_W), and I (CO side-on isomer in S₀), respectively.

Photoexcitation into the singlet manifold initially populates states T₂ and T₁ by ISC within our time resolution; *i.e.* within few femtoseconds according to our scalar-relativistic TDDFT simulations (Table S7). The branching into the two triplet states is estimated from the extinction coefficient of complexes 1 and 2-PF₆ at the pump wavelength. These are 2000 and 12 700 L mol⁻¹ cm⁻¹, respectively, suggesting that for complex 2-PF₆ the absorption of a 400 nm photon results in 2000/12 700 = 16% local excitation of the W-alkyne and 84% of the Ru-bpy chromophore. In both cases these local populations quickly (<100 fs) settle in the corresponding lowest triplet states ³MC_W and ³MLCT_{bpy}, respectively (grey arrows), giving rise to almost instantaneous absorptions at 1945 (ν_{CO} of ³MC_W) and 1904 cm⁻¹ (ν_{CO} of ³MLCT_{bpy}). A detailed analysis of the IR transient at a 0.3 ps pump-probe delay (Fig. S1 in the SI) reveals an additional absorption feature 20 cm⁻¹ red-shifted from the 1904 cm⁻¹ band and covered by the ground-state bleach component. We attribute its origin to a T₂ population trapped in the first excited vibrational state of the CO stretching mode. The ratio of the $\nu = 0 \rightarrow 1$ to $\nu = 1 \rightarrow 2$ band intensities implies that after ISC, 71% of the total population reaches the T₂ state in $\nu = 0$ and 13% in $\nu = 1$ of the CO stretching mode. The population



Table 1 Kinetic parameters for the model of Fig. 7 and line shape parameters for fitting the transient IR absorption spectra of complex 2-PF₆

Species	σ^a	ν_0/cm^{-1b}	$\Delta\nu/\text{cm}^{-1c}$	Rate constant/ ps^{-1}	
T ₂	$\nu = 0$	0.76	1904	27	$k = 0.167, k_0 = 0.033, k_1 = 0.021,$ $k_2 = 0.016, k_3 = 0.0037, k_4 = 0.0083,$ $k_G = 0.0069, k_{10} = 0.16$
	$\nu = 1$	1.52	1884		
T ₁	0.36	1945	35		
I	0.40	1703	21		
G _n	(n + 1)	$\nu_{01} - n \cdot 2\omega_c x_c$	— ^d		

^a integrated cross section relative to σ_{10} of the S₀ CO stretching absorption band. ^b line center. ^c Gaussian line width (FWHM). ^d line shape of the stationary FTIR spectrum.

transfer ${}^3\text{MLCT}_{\text{bpy}} \rightarrow {}^3\text{MC}_w$ applies to both T₂ populations and is described by the rate constant k in eqn (1).

The energy of the T₁ (${}^3\text{MC}_w$) state in Fig. 7 is near the side-on isomer, which allows a T₁ → I transformation with rate constant k_I . This process competes with direct relaxation into the vibrationally excited ground state with $n = 0$ to 3 quanta in the CO stretching mode (rate constants k_0 to k_3 ; higher states are omitted because they were not observed in the IR transients, Fig. 5). Ground state vibrational relaxation is treated in a similar manner as described in the previous section for complex 1. The lifetime of I is so long compared to ground state vibrational relaxation that only the transition into the lowest quantum state $\nu_{\text{CO}} = 0$ of the ground state *via* k_G is considered.

Solving the kinetic equations of this model results in time-dependent populations for all states, from which IR difference absorption spectra are calculated using appropriate line shape functions (for details see SI). Fig. 8 shows a fit to the measured IR transients of Fig. 5c yielding lifetimes and branching ratios as noted in Fig. 7 (corresponding rate constants, relative cross sections, and line shape parameters are summarized in Table 1). Moreover, time traces derived from the model are presented in Fig. 5d–g by blue dashed lines. The agreement between the simulated and measured time and spectral evolutions is excellent, supporting the model used.

The time-dependent concentrations from this kinetic model (see Fig. S2 in the SI) were also used to simulate UV-vis transients based on the calculated electronic spectra. Although this approach neglects the influence of vibrational excitation on the spectrum the simulated transients (Fig. S6b) reproduce the spectro-temporal evolution of the experimental data (Fig. 4a) surprisingly well.

Conclusions

In summary, we investigated the excited state dynamics of the mononuclear alkyne complex 1 and the dinuclear complex 2-PF₆ using femtosecond infrared and UV-vis pump-probe spectroscopy along with quantum chemical calculations. For the reference compound 1, light absorption at 400 nm produces a short-lived (0.25 ps) ${}^3\text{MC}_w$ state, which repopulates the ground state with up to four quanta in the CO stretching mode, subsequently transferring the excess vibrational energy to the solvent on a 10 ps timescale.

The excited state behaviour of the W-CO moiety changes substantially, when its excitation proceeds indirectly.

Photoexcitation of complex 2-PF₆ primarily generates a Ru(bpy)₂ localized ${}^3\text{MLCT}_{\text{bpy}}$ state, which then reacts to a tungsten-centred ${}^3\text{MC}_w$ state. This involves significant charge redistribution in the complex and a rearrangement of the W-C-O geometry. The calculated lifetime for the ${}^3\text{MLCT}_{\text{bpy}} \rightarrow {}^3\text{MC}_w$ reaction derived from semi-classical Marcus theory of $k^{-1} = 2.4$ ps agrees well with the measured time constant of 6 ps. Compared to 1, is the lifetime of the ${}^3\text{MC}_w$ state (12 ps) significantly longer due to a larger S₀- ${}^3\text{MC}_w$ energy gap. The main deactivation channel of the ${}^3\text{MC}_w$ state in 2-PF₆ is inter-system crossing to the ground state, similar to the mononuclear complex. Again, we observe a high level of excitation in the CO stretching mode in the S₀ ground state. In addition, and in contrast to complex 1, we were able to identify a 10% side reaction leading to an intermediate with a CO stretching frequency of 1703 cm⁻¹. Our quantum chemical calculations disclose that this species corresponds to an isomer that is trapped in a metastable state on the S₀ potential surface, with the CO bound side-on to the W centre. To our knowledge, this is the first time that such side-on bound carbonyl complex has been identified experimentally.

Author contributions

D. S. and W. W. S. conceived the idea behind the manuscript. J.-H. B., S. K. B. and K. K. performed the experimental work and spectroscopic studies. S. K. performed the theoretical calculations. The manuscript was written through the contributions of D. S., S. K. and W. W. S. All authors have approved the final version of the manuscript.

Conflicts of interest

There are no conflicts to declare.

Data availability

The data supporting this article have been included in the main manuscript as well as in the supplementary information (SI). Furthermore, all optimized structures and high-resolution images are available *via* the free online repository Zenodo (DOI: [10.5281/zenodo.15083786](https://doi.org/10.5281/zenodo.15083786)). Supplementary information: experimental details of transient absorption spectroscopy, kinetic models and comprehensive computational results. See DOI: <https://doi.org/10.1039/d6sc00998k>.



Acknowledgements

The Financial support from the Deutsche Forschungsgemeinschaft (DFG) via projects SCHW661/4-2 and SE 890/8-1 is gratefully acknowledged. Basic support from the Max Planck Institute for Multidisciplinary Sciences is gratefully acknowledged. All calculations were performed at the Universitätsrechenzentrum of the Friedrich Schiller University Jena.

Notes and references

- 1 F. Calderazzo, in *Encyclopedia of inorganic and bioinorganic chemistry*, ed. R. A. Scott, John Wiley and Sons, Inc, Hoboken, NJ, 2012.
- 2 (a) J. Pospech, I. Fleischer, R. Franke, S. Buchholz and M. Beller, *Angew. Chem., Int. Ed.*, 2013, **52**, 2852; (b) R. Franke, D. Selent and A. Börner, *Chem. Rev.*, 2012, **112**, 5675.
- 3 J. E. Ellis, *Organometallics*, 2003, **22**, 3322.
- 4 (a) M. Finze, E. Bernhardt, H. Willner, C. W. Lehmann and F. Aubke, *Inorg. Chem.*, 2005, **44**, 4206; (b) H. Willner and F. Aubke, *Angew. Chem. Int. Ed. Engl.*, 1997, **36**, 2402.
- 5 W. Unkrig, M. Schmitt, D. Kratzert, D. Himmel and I. Krossing, *Nat. Chem.*, 2020, **12**, 647.
- 6 (a) X. Jin, Y. Bai, Y. Zhou, G. Wang, L. Zhao, M. Zhou and G. Frenking, *Angew. Chem., Int. Ed.*, 2021, **60**, 13865; (b) J. Jin, S. Pan, X. Jin, S. Lei, L. Zhao, G. Frenking and M. Zhou, *Chem.-Eur. J.*, 2019, **25**, 3229; (c) W. Xu, X. Jin, M. Chen, P. Pykkö, M. Zhou and J. Li, *Chem. Sci.*, 2012, **3**, 1548.
- 7 O. T. Summerscales, F. G. N. Cloke, P. B. Hitchcock, J. C. Green and N. Hazari, *Science*, 2006, **311**, 829.
- 8 (a) S. M. Mansell, N. Kaltsoyannis and P. L. Arnold, *J. Am. Chem. Soc.*, 2011, **133**, 9036; (b) P. L. Arnold, Z. R. Turner, R. M. Bellabarba and R. P. Tooze, *Chem. Sci.*, 2011, **2**, 77.
- 9 B. M. Gardner, J. C. Stewart, A. L. Davis, J. McMaster, W. Lewis, A. J. Blake and S. T. Liddle, *Proc. Natl. Acad. Sci.*, 2012, **109**, 9265.
- 10 A. J. Ryan, J. W. Ziller and W. J. Evans, *Chem. Sci.*, 2020, **11**, 2006.
- 11 (a) K. Yuvaraj, J. C. Mullins, T. Rajeshkumar, I. Douair, L. Maron and C. Jones, *Chem. Sci.*, 2023, **14**, 5188; (b) A. Paparo, K. Yuvaraj, A. J. R. Matthews, I. Douair, L. Maron and C. Jones, *Angew. Chem., Int. Ed.*, 2021, **60**, 630.
- 12 P. J. Dyson and J. S. McIndoe, *Transition Metal Carbonyl Cluster Chemistry*, Chapman and Hall/CRC, ProQuest, Boca Raton, Ann Arbor, Michigan, 2018.
- 13 (a) S. Liu, C. E. Plecnik and S. G. Shore, *C. R. Chim.*, 2005, **8**, 1827; (b) I. Castro-Rodriguez and K. Meyer, *J. Am. Chem. Soc.*, 2005, **127**, 11242.
- 14 (a) R. H. Crabtree and M. Lavin, *Inorg. Chem.*, 1986, **25**, 805; (b) F. A. Cotton, *Prog. Inorg. Chem.*, 1976, **21**, 1–28.
- 15 (a) A. F. R. Kilpatrick, J. C. Green and F. G. N. Cloke, *Organometallics*, 2015, **34**, 4816; (b) Y. Takenaka, T. Shima, J. Baldamus and Z. Hou, *Angew. Chem., Int. Ed.*, 2009, **48**, 7888; (c) C. A. Morgan, P. E. Fanwick and I. P. Rothwell, *Inorg. Chim. Acta*, 1994, **224**, 105; (d) R. D. Barr, M. Green, J. A. K. Howard, T. B. Marder, I. Moore and F. A. Stone, *J. Chem. Soc., Chem. Commun.*, 1983, 746; (e) G. A. Carriedo, D. Hodgson, J. A. K. Howard, K. Marsden, F. G. A. Stone, M. J. Went and P. Woodward, *J. Chem. Soc., Chem. Commun.*, 1982, 1006; (f) P. T. Barger and J. E. Bercaw, *J. Organomet. Chem.*, 1980, **201**, C39–C44; (g) A. A. Pasynskii, Y. Skripkin, I. L. Eremenko, V. T. Kalinnikov, G. G. Aleksandrov and Y. Struchkov, *J. Organomet. Chem.*, 1979, **165**, 39; (h) R. Colton, C. J. Commons and B. F. Hoskins, *J. Chem. Soc., Chem. Commun.*, 1975, 363.
- 16 (a) C. Femoni, M. C. Iapalucci, G. Longoni and S. Zacchini, *Dalton Trans.*, 2011, **40**, 8685; (b) X.-Y. Liu, V. Riera, M. A. Ruiz and C. Bois, *Organometallics*, 2001, **20**, 3007; (c) D. G. Dick, Z. Hou and D. W. Stephan, *Organometallics*, 1992, **11**, 2378; (d) D. G. Dick and D. W. Stephan, *Organometallics*, 1990, **9**, 1910; (e) G. M. Dawkins, M. Green, K. A. Mead, J.-Y. Salaün, F. G. A. Stone and P. Woodward, *J. Chem. Soc., Dalton Trans.*, 1983, 527; (f) J. A. Marsella, J. C. Huffman, K. G. Caulton, B. Longato and J. R. Norton, *J. Am. Chem. Soc.*, 1982, **104**, 6360; (g) W. A. Herrmann, M. L. Ziegler, K. Weidenhammer and H. Biersack, *Angew. Chem. Int. Ed. Engl.*, 1979, **18**, 960.
- 17 (a) J. E. Bercaw, E. Rosenberg and J. D. Roberts, *J. Am. Chem. Soc.*, 1974, **96**, 612; (b) C. Krüger and Y.-H. Tsay, *Angew. Chem. Int. Ed. Engl.*, 1973, **12**, 998; (c) K. Jonas, *Angew. Chem. Int. Ed. Engl.*, 1973, **12**, 997.
- 18 (a) A. Gómez-Torres, N. Mavragani, A. Metta-Magaña, M. Murugesu and S. Fortier, *Inorg. Chem.*, 2022, **61**, 16856; (b) S. P. Semproni, C. Milsmann and P. J. Chirik, *Organometallics*, 2012, **31**, 3672; (c) J. F. Corbey, J. H. Farnaby, J. E. Bates, J. W. Ziller, F. Furche and W. J. Evans, *Inorg. Chem.*, 2012, **51**, 7867; (d) T. J. Mueller, M. E. Fieser, J. W. Ziller and W. J. Evans, *Chem. Sci.*, 2011, **2**, 1992; (e) M. Fang, J. E. Bates, S. E. Lorenz, D. S. Lee, D. B. Rego, J. W. Ziller, F. Furche and W. J. Evans, *Inorg. Chem.*, 2011, **50**, 1459; (f) W. H. Monillas, G. P. A. Yap, L. A. MacAdams and K. H. Theopold, *J. Am. Chem. Soc.*, 2007, **129**, 8090; (g) T. E. Hanna, I. Keresztes, E. Lobkovsky and P. J. Chirik, *Inorg. Chem.*, 2007, **46**, 1675; (h) W. A. Chomitz and J. Arnold, *Chem. Commun.*, 2007, 4797; (i) P. J. Chirik, L. M. Henling and J. E. Bercaw, *Organometallics*, 2001, **20**, 534; (j) H. Basch, D. G. Musaev, K. Morokuma, M. D. Fryzuk, J. B. Love, W. W. Seidel, A. Albinati, T. F. Koetzle, W. T. Klooster, S. A. Mason and J. Eckert, *J. Am. Chem. Soc.*, 1999, **121**, 523; (k) M. D. Fryzuk, J. B. Love, S. J. Rettig and V. G. Young, *Science*, 1997, **275**, 1445; (l) J. D. Queen, A. Rajabi, Q. E. Goudzwaard, Q. Yuan, D. K. Nguyen, J. W. Ziller, F. Furche, Z. Xi and W. J. Evans, *Chem. Sci.*, 2024, **15**, 16069.
- 19 M. S. Batov, H. T. Partlow, L. Chatelain, J. A. Seed, R. Scopelliti, I. Zivkovic, R. W. Adams, S. T. Liddle and M. Mazzanti, *Nat. Chem.*, 2025, **17**, 1425.
- 20 (a) Q. Zhuo, X. Zhou, T. Shima and Z. Hou, *Angew. Chem., Int. Ed.*, 2023, **62**, e202218606; (b) D. Singh, W. R. Buratto, J. F. Torres and L. J. Murray, *Chem. Rev.*, 2020, **120**, 5517;



- (c) R. J. Burford, A. Yeo and M. D. Fryzuk, *Coord. Chem. Rev.*, 2017, **334**, 84.
- 21 (a) V. Vorobyev, A. A. Mikhailov, V. Y. Komarov, A. N. Makhinya and G. A. Kostin, *New J. Chem.*, 2020, **44**, 4762; (b) B. Cormary, S. Ladeira, K. Jacob, P. G. Lacroix, T. Woike, D. Schaniel and I. Malfant, *Inorg. Chem.*, 2012, **51**, 7492; (c) D. V. Fomitchev, I. Novozhilova and P. Coppens, *Tetrahedron*, 2000, **56**, 6813; (d) M. S. Lynch, M. Cheng, B. E. van Kuiken and M. Khalil, *J. Am. Chem. Soc.*, 2011, **133**, 5255.
- 22 T. E. Bitterwolf, *Coord. Chem. Rev.*, 2006, **250**, 1196.
- 23 (a) S. Kundu, P. N. Phu, P. Ghosh, S. A. Kozimor, J. A. Bertke, S. C. E. Stieber and T. H. Warren, *J. Am. Chem. Soc.*, 2019, **141**, 1415; (b) E. I. Tocheva, F. I. Rosell, A. G. Mauk and M. E. P. Murphy, *Science*, 2004, **304**, 867.
- 24 M. Wrighton, *Chem. Rev.*, 1974, **74**, 401.
- 25 (a) J. J. Turner, M. W. George, M. Poliakoff and R. N. Perutz, *Chem. Soc. Rev.*, 2022, **51**, 5300; (b) K. Ramasesha, D. R. Carlson and S. Bandaranayake, *Chem. Phys. Rev.*, 2025, **6**, 21307; (c) A. Schori, E. Biasin, A. Banerjee, S. Boutet, P. H. Bucksbaum, S. Carbajo, K. J. Gaffney, J. M. Glowonia, R. Hartsock, K. Ledbetter, A. Kaldun, J. E. Koglin, K. Kunnus, T. J. Lane, M. Liang, M. P. Minitti, J. T. O'Neal, R. M. Parrish, F. Poitevin, J. M. Ruddock, S. Nelson, B. Stankus, P. M. Weber, T. J. A. Wolf, M. Odelius and A. Natan, *Nat. Commun.*, 2025, **16**, 4767; (d) R. M. Jay, M. R. Coates, H. Zhao, M.-O. Winghart, P. Han, R.-P. Wang, J. Harich, A. Banerjee, H. Wikmark, M. Fondell, E. T. J. Nibbering, M. Odelius, N. Huse and P. Wernet, *J. Am. Chem. Soc.*, 2024, **146**, 14000; (e) J. Troß, J. E. Arias-Martinez, K. Carter-Fenk, N. C. Cole-Filipiak, P. Schrader, L. M. McCaslin, M. Head-Gordon and K. Ramasesha, *J. Am. Chem. Soc.*, 2024, **146**, 22711; (f) S. A. Trushin, K. Kosma, W. Fuß and W. E. Schmid, *Chem. Phys.*, 2008, **347**, 309; (g) W. Fuß, S. A. Trushin and W. E. Schmid, *Res. Chem. Intermed.*, 2001, **27**, 447.
- 26 (a) R. Feng, E. D. Glendening and K. A. Peterson, *Inorg. Chem.*, 2020, **59**, 4753; (b) Z. Zhang, Q. Li, Y. Xie, R. B. King and H. F. Schaefer, *J. Phys. Chem. A*, 2010, **114**, 4672.
- 27 M. Hüttenschmidt, H. Lange, M. A. A. Cordero, A. Villinger, S. Lochbrunner and W. W. Seidel, *Dalton Trans.*, 2022, **51**, 852.
- 28 J. Franz, M. Oelschlegel, J. P. Zobel, S.-A. Hua, J.-H. Bortler, L. Schmid, G. Morselli, O. S. Wenger, D. Schwarzer, F. Meyer and L. González, *J. Am. Chem. Soc.*, 2024, **146**, 11272.
- 29 T. P. Dougherty and E. J. Heilweil, *Chem. Phys. Lett.*, 1994, **227**, 19.
- 30 (a) D. Schwarzer, J. Troe, M. Votsmeier and M. Zerezke, *J. Chem. Phys.*, 1996, **105**, 3121; (b) J. C. King, J. Z. Zhang, B. J. Schwartz and C. B. Harris, *J. Chem. Phys.*, 1993, **99**, 7595.
- 31 B. Schluschaß, J.-H. Bortler, S. Rupp, S. Demeshko, C. Herwig, C. Limberg, N. A. Maciulis, J. Schneider, C. Würtele, V. Krewald, D. Schwarzer and S. Schneider, *JACS Au*, 2021, **1**, 879.
- 32 D. Schwarzer, J. Troe and M. Zerezke, *J. Chem. Phys.*, 1997, **107**, 8380.
- 33 (a) J. Yardley, *Introduction to Molecular Energy Transfer*, Elsevier Science, Burlington, 2012; (b) L. Landau and E. Teller, *Phys. Z. Sowjetunion*, 1936, **10**, 34.
- 34 P. Hamm, S. M. Ohline and W. Zinth, *J. Chem. Phys.*, 1997, **106**, 519.
- 35 (a) A. El Nahhas, C. Consani, A. M. Blanco-Rodríguez, K. M. Lancaster, O. Braem, A. Cannizzo, M. Towrie, I. P. Clark, S. Zálíš, M. Chergui and A. Vlček, JR., *Inorg. Chem.*, 2011, **50**, 2932; (b) R. Fernández-Terán and L. Sévery, *Inorg. Chem.*, 2021, **60**, 1334; (c) L. Chen, A. M. McKillop, A. P. Fidler and M. L. Weichman, *Nanophotonics*, 2025, **14**, 5437.
- 36 (a) A. C. Bhasikuttan, M. Suzuki, S. Nakashima and T. Okada, *J. Am. Chem. Soc.*, 2002, **124**, 8398; (b) O. Bräm, F. Messina, A. M. El-Zohry, A. Cannizzo and M. Chergui, *Chem. Phys.*, 2012, **393**, 51.
- 37 S. Wallin, J. Davidsson, J. Modin and L. Hammarström, *J. Phys. Chem. A*, 2005, **109**, 4697.
- 38 G. Yang, G. E. Shillito, C. Zens, B. Dietzek-Ivanšić and S. Kupfer, *J. Chem. Phys.*, 2023, **159**, 24109.
- 39 G. Yang, L. Blechschmidt, L. Zedler, C. Zens, K. Witas, M. Schmidt, B. Esser, S. Rau, G. E. Shillito, B. Dietzek-Ivanšić and S. Kupfer, *Chem.-Eur. J.*, 2025, **31**, e202404671.
- 40 (a) A. Solé-Daura and F. Maseras, *Chem. Sci.*, 2024, **15**, 13650; (b) A. Koch, D. Kinzel, F. Dröge, S. Gräfe and S. Kupfer, *J. Phys. Chem. C*, 2017, **121**, 16066.
- 41 S. Bai, P. Zhang and D. N. Beratan, *J. Phys. Chem. A*, 2024, **128**, 5721.
- 42 H. Vennekate, A. Walter, D. Fischer, J. Schroeder and D. Schwarzer, *Z. Phys. Chem.*, 2011, **225**, 1089.
- 43 A. J. Blake, R. W. Cockman, E. A. V. Ebsworth and J. H. Holloway, *J. Chem. Soc., Chem. Commun.*, 1988, 529.
- 44 (a) J. Foerstner, A. Kakoschke, R. Wartchow and H. Butenschön, *Organometallics*, 2000, **19**, 2108; (b) L.-K. Liu, K.-Y. Chang and Y.-S. Wen, *J. Chin. Chem. Soc.*, 1997, **44**, 33; (c) M. C. Azar, M. J. Chetcuti, C. Eigenbrot and K. A. Green, *J. Am. Chem. Soc.*, 1985, **107**, 7209; (d) K. Hoffmann and E. Weiss, *J. Organomet. Chem.*, 1977, **128**, 399; (e) W. Wong, S. J. Singer, W. D. Pitts, S. F. Watkins and W. H. Baddley, *J. Chem. Soc., Chem. Commun.*, 1972, 672.

